Science of the Total Environment 825 (2022) 153784

Contents lists available at ScienceDirect

Science of the Total Environment

journal homepage: www.elsevier.com/locate/scitotenv

Diel variations in chemical and isotopic compositions of a stream on King George Island, Antarctica: Implications for hydrologic pathways of meltwater

Hyejung Jung [a], Sung-Wook Jeen [b,c], Hyoungseok Lee [d], Jeonghoon Lee [a,*]

[a] Department of Science Education, Ewha Womans University, Seoul 03760, Republic of Korea
[b] Department of Earth and Environmental Sciences, Jeonbuk National University, Jeonju 54907, Republic of Korea
[c] Department of Environment and Energy, Jeonbuk National University, Jeonju 54907, Republic of Korea
[d] Division of Life Sciences, Korea Polar Research Institute (KOPRI), Incheon 21990, Republic of Korea

HIGHLIGHTS

- Stable water isotopes are valuable tools for studying the origin and flowpath of water.
- Melt rate differences result in diel variations by the isotopic exchange.
- Diel isotope signal is observed during summer periods by runoff flowpath.
- When the flow increases, the EC values decrease by the dilution effect.
- The results can help to understand hydrologic pathways for climate-related change.

GRAPHICAL ABSTRACT

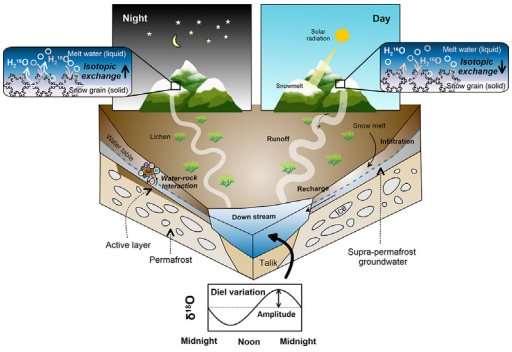

ARTICLE INFO

Article history:
Received 18 November 2021
Received in revised form 20 January 2022
Accepted 6 February 2022
Available online 16 February 2022

Editor: Christian Herrera

Keywords:
Permafrost hydrology
Hydrological environment
Stable water isotopes
Diel variation
Active layer
Antarctica

ABSTRACT

Antarctica is highly susceptible to climate and environmental change. In particular, climate change can lead to the warming of permafrost and the development of active layers in permafrost areas, resulting in variations in hydrological characteristics. This study investigated the hydrological process associated with a stream in a snow-dominated headwater catchment on King George Island, maritime Antarctica, during austral summer using the chemical and isotopic compositions. During the cold period, as the snowmelt rate decreased, the amount of new water also decreased. Hence, the electrical conductivity (EC) increased because the contribution of supra-permafrost groundwater ("old" water), which occurs in the active layer, increased more during the cold period than during the warm period. Moreover, diel variations in the stable isotopic compositions ($\delta^{18}O$ and δD) of snowmelt ("new" water) were clearly observed in the stream water, indicating that runoff was the dominant flow path of snowmelt during the cold period. In contrast, during the warm period, the amount of snowmelt increased and the EC value decreased as a result of the dilution effect. In addition, compared with the cold period, diel variations in the isotopic compositions of the stream water were attenuated during the warm period. This attenuation effect was not due to the increased contribution of old water; instead, it was due to the contribution of new water with a low-amplitude signal in the diel variations of the isotopic compositions. Thus, the observed diel variations in the isotopic compositions of the stream water during cold and warm periods suggest that this catchment is dominated by new water. These findings are helpful for improving our understanding of climate-related changes in the hydrological pathways and water-related ecosystems of polar catchments.

* Corresponding author.
E-mail address: jeonghoon.d.lee@gmail.com (J. Lee).

http://dx.doi.org/10.1016/j.scitotenv.2022.153784

1. Introduction

Antarctica is highly vulnerable to climate and environmental change (Stammerjohn and Scambos, 2020). In particular, climate change can lead to the warming of permafrost and increase the thickness of the active layer in permafrost areas (Biskaborn et al., 2019), resulting in changes in hydrogeological characteristics (Qiu, 2012). The active layers are topsoil layers that repeatedly thaw and freeze depending on the temperature, and can melt up to the permafrost table (Woo, 2012). The flux and depth of the supra-permafrost groundwater that occurs in the active layer increase with the deepening of the active layer during summer (Sjöberg et al., 2021), whereas the frozen active layer functions as an aquitard that limits the infiltration of meltwater during winter (Cooper et al., 1991). Hydrological processes involving solute transport can vary depending on the dynamics of the active layers in permafrost regions (Langford et al., 2020). These changes in hydrological and solute transport processes affect Antarctic terrestrial vegetation such as lichens and mosses. The supra-permafrost groundwater flowing within the active layers is a key water source for lichen and moss species and a notable component that helps maintain terrestrial ecosystems in Antarctica (Kim et al., 2020b). The distribution and abundance of vegetation are related to water availability in the Antarctic terrestrial environment (Kennedy, 1993; Leishman and Wild, 2001; Cho et al., 2020). Thus, it is necessary to monitor the current hydrologic characteristics of Antarctic regions to understand the changes in local hydrological processes and the response of Antarctic terrestrial ecosystems to global warming.

As natural tracers, stable water isotopes ($\delta^{18}O$ and δD) have proven to be valuable tools for studying the origin and flow path of water in catchment hydrology (McGuire and McDonnell, 2007; Klaus and McDonnell, 2013; Kim et al., 2017a; Jung et al., 2020a, 2021). In particular, the stable isotopic compositions of snow and ice are useful tools for investigating the contribution of "new" water (meltwater) and "old" water (supra-groundwater and groundwater) in snow-dominated headwater catchments and glacial river systems (Engel et al., 2016; Cano-Paoli et al., 2019). When new water moves to a stream through the direct pathway of runoff, the isotopic and chemical signals of this new water are transmitted downstream. In contrast, the indirect pathway through which new water infiltrates through the soil layer and is discharged as old water can undergo evaporation, resulting in different isotopic values from the original snowmelt. Additionally, chemical tracers such as solute concentrations or electrical conductivity (EC) can provide important clues regarding the hydrochemical and solute transport processes. Chemical tracers are also helpful for understanding chemical weathering under different flow path dynamics (Cano-Paoli et al., 2019). These environmental tracers have been proposed to complement traditional hydrological information over the past decades (Cano-Paoli et al., 2019) to separate flow components (Mook et al., 1974; Sklash et al., 1976; Kirchner et al., 2004; Muñoz-Villers and McDonnell, 2012; Kim et al., 2017a) or estimate mean catchment residence times (McGuire and McDonnell, 2006; Birkel et al., 2012; Tetzlaff et al., 2018; Cano-Paoli et al., 2019; Jung et al., 2020b).

During the snowmelt season in polar environments, the daily flows of stream water and supra-permafrost groundwater are responsive to the day–night energy cycle (Engel et al., 2016). The diel variations in these flows are the result of changes in the snowmelt rate due to the fluctuation in the air temperature; specifically, the increasing air temperature during the day leads to an increase in the snowmelt rate, and thus, higher meltwater discharge. Differences in the snowmelt rate then result in a diel variation in the stable isotopic composition of meltwater corresponding to the degree of isotopic exchange between water and ice (Taylor et al., 2001). At a high snowmelt rate, there is insufficient time for the isotopic exchange reaction between liquid water and solid ice, resulting in meltwater that is relatively depleted in ^{18}O (Taylor et al., 2001; Lee et al., 2010a). In contrast, ^{18}O-enriched meltwater is generated at a low snowmelt rate because there is sufficient time for the isotopic exchange reaction (Taylor et al., 2001; Lee et al., 2010a). Thus, the day–night energy cycle gives rise to differences in the snowmelt rate, which result in the diel variation in the stable isotopic composition of meltwater (i.e., relatively depleted during the day and enriched during the night) (Lee et al., 2020).

To understand the variations in the hydrological processes occurring within dynamic active layers, high-frequency sampling must be performed to match the timescale of the catchment hydrological response (Kirchner et al., 2004). Numerous studies have investigated the hydrologic characteristics of headwater catchments in glacial regions using diel variations, thus emphasizing the importance of studies on high-frequency sampling; however, few studies have investigated hydrological pathways based on daily-scale field data in polar environments (Throckmorton et al., 2016). Based on the diel variation in the isotopic composition of stream water, Lee et al. (2020) characterized for the first time the hydrological processes of the Barton Peninsula on King George Island (KGI), Antarctica. Based on Lee et al. (2020), the present study aims to clarify the hydrologic flow path by investigating the diel variations in the chemical and isotopic compositions of stream water on KGI. Considering existing reports (Tetzlaff et al., 2018; Langford et al., 2020; Lee et al., 2020; Fouché et al., 2021), we hypothesize that the groundwater flow gradually increases with an increase in the active layer thickness during summer in permafrost regions. Accordingly, this study investigates the flow paths in Antarctica and examines the consistency of these results with those of existing studies undertaken in permafrost regions. In particular, dynamic hydrological processes are examined by analyzing snow, supra-permafrost groundwater, and stream samples obtained from January 12 to 29, 2020 (i.e., austral summer).

2. Study area and methods

2.1. Study site

Located 120 km off the north coast of the Antarctic Peninsula, KGI is a volcanic island of the South Shetland Islands (61°50′–62°15′ S, 57°30′–59°01′ W) (Lee et al., 2020). The surface area of KGI is approximately 1310 km^2 (Lim et al., 2014) and most of the island (~95%) is covered by glaciers (Chang et al., 1990). The study area is located in the coastal area near the Korean research station (King Sejong) on the Barton Peninsula at the southwestern end of KGI (Fig. 1a). The highest peak on the Barton Peninsula is Noel Hill (255 m), 2 km northeast of it, which is covered with ice all year round (Chang et al., 1990). The southwest coast of the Barton Peninsula is partially steeply sloped, and most of it has relatively wide and gentle slopes with elevations of 90–180 m above sea level, except for the peaks (Lee et al., 2004).

The Barton Peninsula is geologically composed of volcanic sedimentary rocks (Sejong Formation) in the lower part, and calc-alkaline volcanic and igneous rocks in the upper part (Yoo et al., 2001). The Sejong Formation is approximately 100 m thick and consists of various conglomerate and sandstone beds intercalated with lapilli tuffs (Yoo et al., 2001). The Sejong Formation dates to the Late Paleocene–Eocene (Chun et al., 1994). In the upper part of the formation, mafic to intermediate volcanic lavas are broadly distributed on the Barton Peninsula (Lee et al., 2004). They are mostly basaltic andesites, with rare massive andesites (Lee et al., 2001). Several units of thick layers of lapilli tuff are intercalated with lava flows, and it is likely that most of the lava erupted during the Paleocene and Eocene (Pankhurst and Smellie, 1983; Smellie et al., 1984; Kim et al., 2000a; Hur et al., 2001; Lee et al., 2004). In the central northwestern area of the Barton Peninsula, granite diorite stocks with a small mass of fine-grained diorites intruded during the Eocene (Park, 1989; Lee et al., 1996; Kim et al., 2000a).

The region of KGI has a cold and humid oceanic climate (Lee et al., 2020). According to the weather data for the study area measured at the King Sejong Station during the study month (January 2020), the average values of temperature, relative humidity, and total precipitation are 4.8 ± 3.2 °C, 84.3 ± 16.6%, and 7.8 mm, respectively, while the average wind speed is 5.0 ± 2.9 m/s, primarily in the northwest and northeast directions. According to Falk et al. (2018), the snow depth on the Barton Peninsula ranged from 0 up to 2 m during the austral summer from 2011

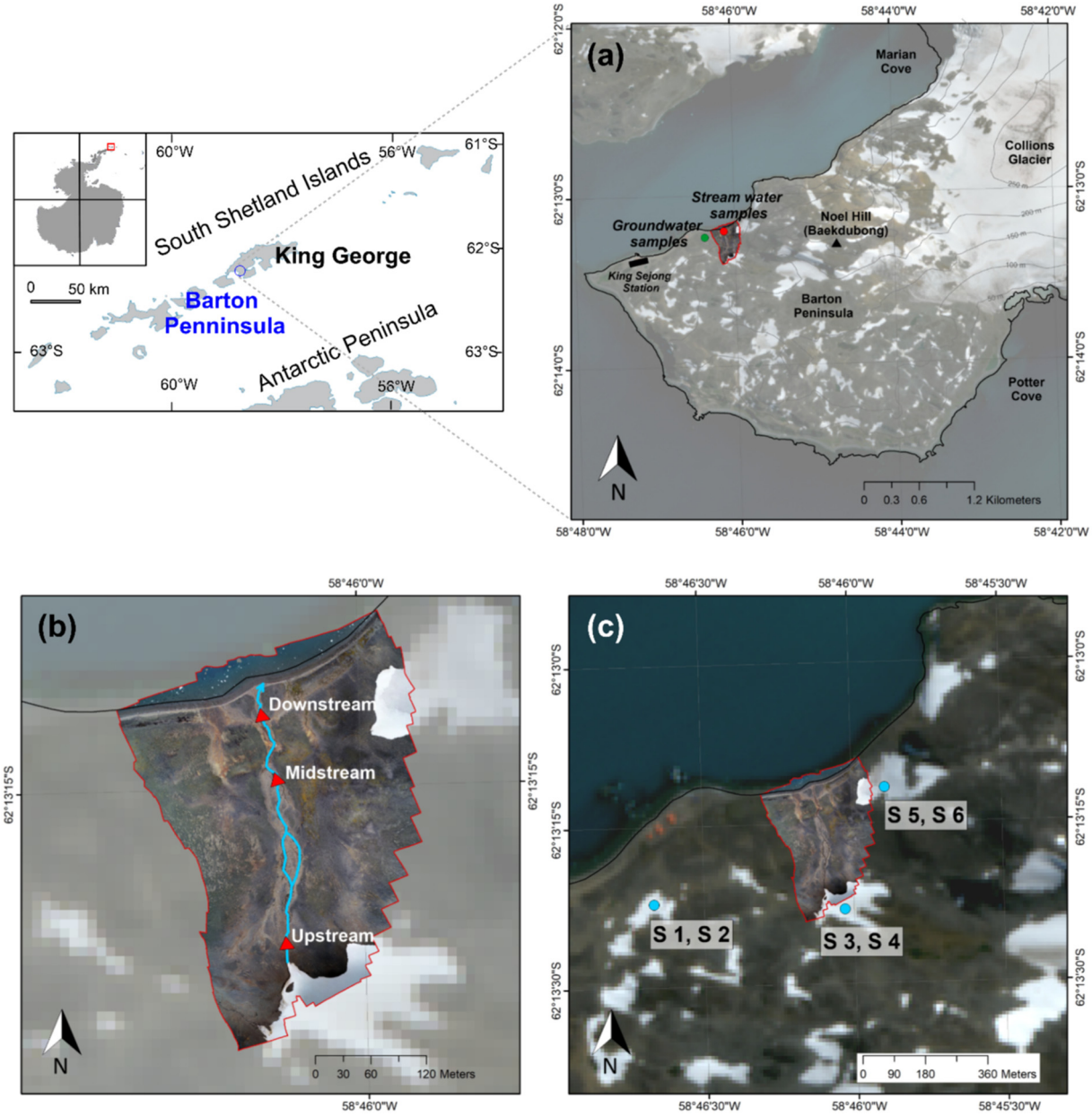

Fig. 1. (a) Locations of the stream water and groundwater sampling sites near King Sejong Station in Antarctica; (b) photograph of sampling sites of stream water, obtained by a drone; and (c) map showing the snow sampling sites and image of snow cover around the stream observed by Sentinel-1 satellite on January 19, 2020.

to 2016. The mean thaw depth has been observed to be 60 cm in Bellingshausen, KGI (2008–2016) (Hrbáček et al., 2021). The study site considered in this study is a small stream in a snow-dominated headwater catchment located approximately 1 km from King Sejong Station on KGI (Fig. 1a). The stream is approximately 315 m long, with a gentle hill slope (average slope of 13°). The study site is composed of fine sand and poorly sorted soil, and the hydraulic conductivity of the sediments ranges from 3.0×10^{-6} m/s to 4.1×10^{-5} m/s (Kim et al., 2020b).

2.2. Sample collection and field observations

A total of 77 samples, including stream water ($n = 52$), snow ($n = 6$), and supra-permafrost groundwater ($n = 19$) samples, were obtained from January 12 to 29, 2020, for chemical and isotopic analyses to understand the hydrological processes in the study region. The sampling locations are shown in Fig. 1. The groundwater samples were collected from a nearby stream using an installed piezometer (Fig. 1a). Details of the groundwater sampling method can be found in Kim et al. (2020b). The stream water samples were collected from the upstream, midstream, and downstream regions only once on the first sampling day (January 12, 2020), whereas they were collected two to four times per day in the downstream region from January 13 to January 29, 2020 (Fig. 1b). The snow samples were collected from the surface of the upstream region and around the stream (Fig. 1c). They were placed in plastic bags and allowed to melt in the laboratory at the King Sejong Station. The meltwater samples were stored in high-density polyethylene (HDPE) bottles in the field and kept frozen until analysis. All samples were collected while walking from the King Sejong Station to the sampling site. For the stream water samples, high-frequency sampling was performed while walking a 2 km round-trip several times a day to investigate the diel variations in the stream water. For all samples, the EC and temperature (T) were measured using an EC probe (Thermo Scientific Orion Star™ A223, USA). Additionally, streamflow velocity was measured in situ using a flow watch (JDC Electronic SA, Switzerland). Meteorological data, specifically, the air temperature and relative humidity,

recorded every 10 min at the King Sejong Station, were acquired from the Korea Polar Research Institute (KOPRI). Other data (cloud cover, precipitation, and wind speed), recorded every 6 h at King Sejong Station, were obtained from a publicly available website (https://rp5.ru). The soil temperature at a depth of 15 cm was measured using a 105 T thermocouple probe with an accuracy of ±0.1 °C at the stream.

2.3. Sample analyses

All water samples were collected in 15 mL HDPE bottles (Tarsons, India) without head space, and were filtered through 0.45-μm syringe filters (Mixed Cellulose Esters, ADVANTEC, Toyo Roshi Kaisha Ltd.) for cation, anion, and isotope analyses. For cation analysis, water samples were acidified to pH < 2 using ultrapure nitric acid (HNO_3) (Sigma-Aldrich, USA). Then, the samples were shipped frozen to the Seoul Center of the Korea Basic Science Institute for cation analysis using inductively coupled plasma–atomic emission spectroscopy (ICP–AES; Jobin Yvon Horiba Ultima 2, Milan, Italy). Five cations (Ca, Mg, Na, K, and Si) were measured in triplicate for each sample. After the analysis was completed, the peak of the sample was checked to see if it was the same as that of the standard material. A set of multi-element standard solutions were prepared for calibration using ICP–AES. For calibration, a solution containing a known amount of each element was measured. The anions were analyzed using ion chromatography (ICS-90; Dionex, Sunnyvale, CA, USA) and Chromeleon™ software (Thermo Fisher Scientific, CA, USA) at Jeonbuk National University (precision at the 95% confidence level).

The stable isotopic compositions ($\delta^{18}O$ and δD) of the water samples were analyzed at Ewha Womans University (Seoul, Korea) using an L2140-i isotopic water–liquid analyzer (Picarro Inc., Sunnyvale, CA, USA) through wavelength-scanned cavity ring-down spectroscopy (WSCRDS). For external calibration, three international measurement standards were considered: the second Vienna Standard Mean Ocean Water (VSMOW2) ($\delta^{18}O$: 0.0‰ and δD: 0.0‰), Greenland Summit Precipitation (GRESP) ($\delta^{18}O$: −33.39‰ and δD: −257.8‰), and Standard Light Antarctic Precipitation 2 (SLAP2) ($\delta^{18}O$: −55.50‰ and δD: −427.5‰). The reproducibility of the measurements was calculated to be <1.0 per mil for δD and 0.1 per mil for $\delta^{18}O$.

The stable isotopic results were expressed in delta notation (δ) in units of per mil (‰) relative to the international reference standard, following Eq. (1):

$$\delta(‰) = \left\{ \left(\frac{R_{sample}}{R_{standard}} \right) - 1 \right\} \times 1000 \quad (1)$$

where R denotes the ratio of heavy to light isotopes ($^2H/^1H$, $^{18}O/^{16}O$), and R_{sample} and $R_{standard}$ are the isotopic ratios in the sample and standard, respectively. The $^2H/^1H$ and $^{18}O/^{16}O$ ratios are expressed as δD and $\delta^{18}O$, respectively, with respect to VSMOW.

3. Results

3.1. Hydrometeorological observations

On the first day (January 12, 2020), the flow velocities measured in the upstream, midstream, and downstream regions were 0.7 m/s, 0.8 m/s, and 1.2 m/s, respectively, thus increasing from upstream to downstream. The water temperature on the same day exhibited similar values of 2.6 °C, 2.8 °C, and 2.9 °C in the upstream, midstream, and downstream regions, respectively. From the second day, in situ measurements were performed only in the downstream region. Fig. 2a presents the temporal variations in the streamflow in the downstream region during the study period.

The flow velocity in the stream was highly dynamic and exhibited daily increasing and decreasing patterns with an average value of 0.84 ± 0.38 m/s. For example, on the afternoon of January 12, 2020, when sampling was initiated, the flow velocity was 1.2 m/s, which sharply decreased to 0.3 m/s on the morning of January 13. On the same night, the flow velocity increased to 0.91 m/s before gradually decreasing to a minimum of 0.24 m/s on January 18. Subsequently, low flow was maintained until January 22 when it increased again before peaking at 1.58 m/s on January 28 (Fig. 2a). Although the amplitudes of the flow velocities were different, regular diel variations with the day–night cycle were observed. According to the in situ measurements, the minimum and maximum flows were observed in the morning and late evening, respectively.

The total precipitation during the study period was 1.55 mm (Fig. 2a), with eight rainfall events, most of which corresponded to drizzle (0.05–0.1 mm) over <6 h. However, relatively intense rainfall of 1 mm occurred from 14:00 on January 28 to 02:00 on January 29, 2020, and the maximum streamflow was recorded at this time. The soil water content ranged from 0.11 m^3/m^3 to 0.17 m^3/m (average of 0.12 ± 0.01 m^3/m^3, Fig. 2a) and responded sensitively to rainfall events.

The air temperature ranged from −4.0 °C to 16.8 °C, with an average of 4.8 ± 3.2 °C (Fig. 2b). The temperature was primarily above 0 °C, excluding that in the dawn hours of January 16, 18, 19, and 20, 2020, because it was austral summer (Fig. 2b). The flow velocity of the stream followed the diel variations in air temperature and rainfall (Fig. 2a and b). In general, air temperature is the dominant parameter influencing the snowmelt rate (Hinkler et al., 2008; Rango and Martinec, 1995; Hussainzada et al., 2021b). An increase in air temperature led to a higher discharge, and the return to freezing temperatures was associated with an extended recession (Paquette et al., 2018). The water temperature of the stream fluctuated less than the air temperature, ranging from 1.9 °C to 5.6 °C (average of 3.28 ± 0.8 °C, Fig. 2b). The soil temperature ranged from 1.5 to 8.3 °C (average of 4.7 ± 1.1 °C, Fig. 2b).

The relative humidity ranged from 33.5% to 100% (average of 84.3 ± 16.6%, Fig. 2c), and the cloud cover ranged from 20% to 100% (average of 85 ± 17%, Fig. 2c). During the study period, high cloud coverage (> 75%) was observed almost every day, except on January 18 and 19, 2020. The variation in the wind direction is shown in Fig. 2d. The wind directions were divided into 16 sectors, considering the east (E; 90°), south (S; 180°), west (W; 270°), and north (E; 360°) directions in a clockwise manner. During the study period, the E–NE (65°) sector corresponded to the highest frequency of 16%, followed by the E (90°), W–NW (295°), and NW (315°) sectors with values of 11%. In general, the wind direction is closely related to the air temperature and humidity. From January 17 to 19, E and E–NE winds with cold and dry characteristics from the Weddell Sea prevailed (Fig. 2d). The wind speed ranged from 0 m/s to 12.0 m/s (average of 5.0 ± 2.9 m/s), and at high wind speeds of ≥8 m/s, N, E, and NE winds accounted for more than 80% of all wind directions (Fig. 2d).

We divided the study period into three sub-periods (see below) based on the hydrometeorological variables (air temperature and flow velocity) to examine the hydrological pathways according to changes in the temperature-sensitive active layer. The meteorological and hydrological variables for each of the following sub-periods are summarized in Table 1. (1) Period 1, January 12–14, 2020: increasing mid-flow (0.9 ± 0.3 m/s) with warm temperatures (5.4 ± 3.0 °C); (2) Period 2, January 15–21, 2020: decreasing flow (0.5 ± 0.3 m/s) and cold with a large diurnal air temperature difference (4.5 ± 4.1); and (3) Period 3, January 22–29, 2020: increasing flow (1.1 ± 0.3 m/s) and mild with a small diurnal air temperature difference (4.8 ± 2.3 °C).

3.2. Chemical characteristics of stream water, groundwater, and snow

Table S1 lists details of the snow and groundwater sampling, in-situ water quality measurements. Table S2 lists the physical and chemical properties of the stream water in the study area. The EC values of the groundwater (n = 19), stream water (n = 52), and snow (n = 6) samples were 88.91–665.5 μS/cm (270.33 ± 153.26 μS/cm), 30.16–64.92 μS/cm (48.90 ± 9.31 μS/cm), and 2.85–47.13 μS/cm (average of 19.52 ± 20.56 μS/cm), respectively. The EC of groundwater was significantly higher than that of snow and stream water (t-test, $p < 0.05$), suggesting that the chemical composition of groundwater was significantly affected by water–rock interactions. The EC values of the stream samples were

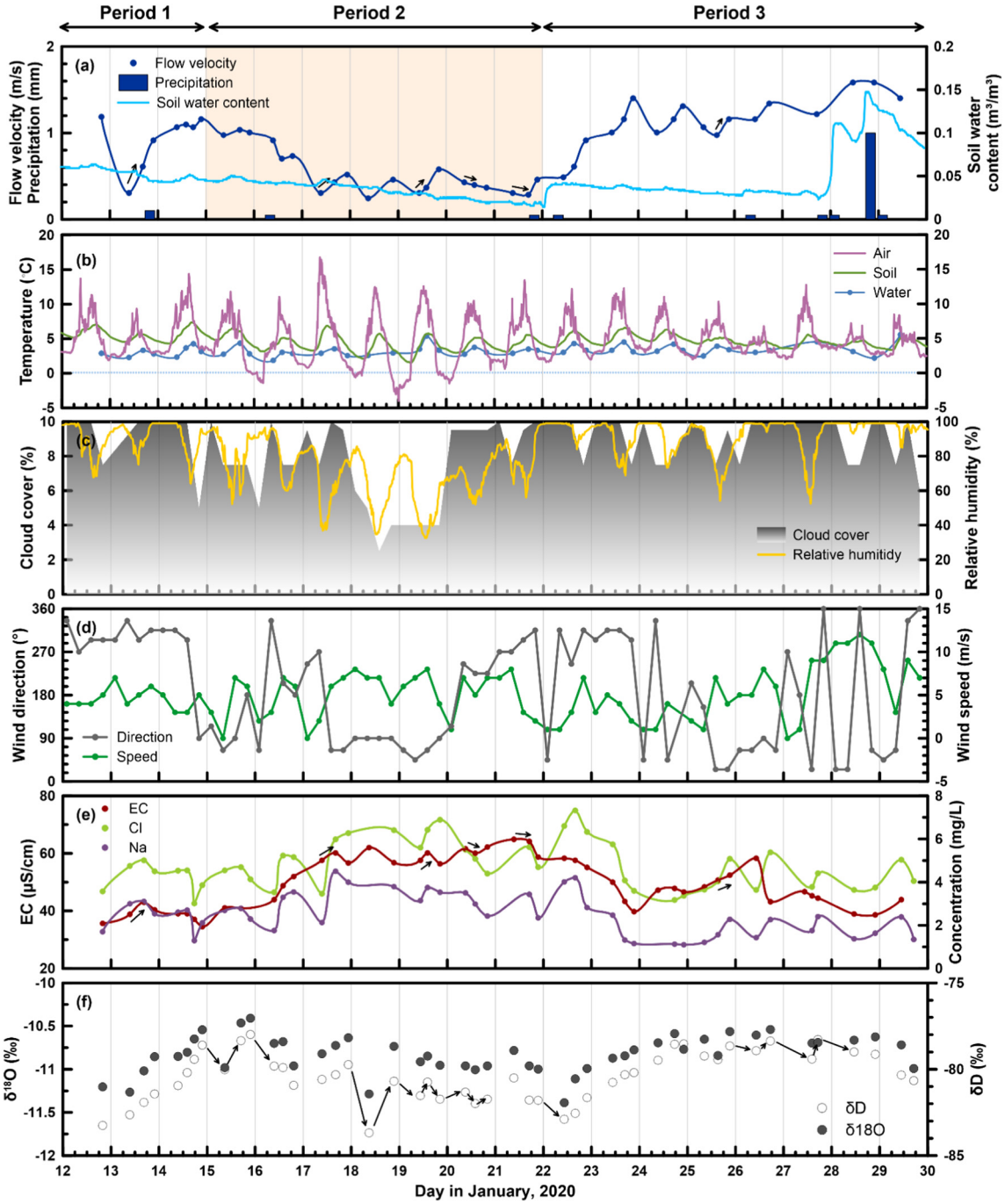

Fig. 2. (a) Timeseries of flow velocity, precipitation, and soil water content; (b) air temperature, soil temperature, and water temperature; (c) cloud cover and relative humidity; (d) wind direction and wind speed; (e) Cl and Na concentrations and EC; and (f) stable isotopic compositions of stream water.

intermediate to those of snow and groundwater. For the stream samples, the average concentrations of Ca^{2+}, Mg^{2+}, K^{+}, and Na^{+}, were 0.68 ± 0.39 mg/L, 0.46 ± 0.14 mg/L, 0.40 ± 0.27 mg/L, and 2.51 ± 0.92 mg/L, respectively. The average Si concentration, which is one of the major elements, in the stream water was 0.33 ± 0.17 mg/L (range of 0.15–1.01 mg/L). The average concentrations of Cl^{-}, SO_4^{2-}, and NO_3^{-} in the stream samples were 4.76 ± 1.07 mg/L, 6.35 ± 1.84 mg/L, and 0.14 ± 0.09 mg/L, respectively. F^{-} was not detected. Fig. 2e shows the temporal variations in the EC values and Na^{+} and Cl^{-} concentrations in the stream water. The EC values were positively correlated with Na^{+} (correlation coefficient, $r = 0.49$) and Cl^{-} concentrations ($r = 0.54$), whereas they were negatively correlated with flow velocity ($r = -0.68$). The chemical characteristics of the stream water for each period are summarized in Table 2. Overall, the EC values and Na^{+} and Cl^{-} concentrations were higher in Period 2, when the average air temperature and flow velocity were lower than those in Periods 1 and 3.

3.3. Isotopic characteristics of stream water, groundwater, and snow

The $\delta^{18}O$ and δD values of the stream water samples ($n = 52$) ranged from −11.4‰ to −10.4‰ and from −84.0‰ to −78.0‰, respectively. The average and standard deviation for oxygen and hydrogen were − 10.8 ± 0.2‰ and − 80.6 ± 1.6‰, respectively. The $\delta^{18}O$ values of the snow ($n = 6$) and groundwater ($n = 19$) samples ranged from −12.1‰ to −7.0‰ (average of −10.4 ± 1.9‰) and from −12.2‰ to −10.4‰ (average of −11.4 ± 0.4‰), respectively, while the δD values ranged from −88.7‰

Table 1
Hydrometeorological variables in each period from 12 January 2020 to 29 January 2020.

Hydrometeorological variables	Flow velocity				Water temperature				Air temperature			Relative humidity			Soil temperature			Total precipitation
Unit	m/s				˚C				˚C			%			˚C			mm
Sampling period	*n*	Min	Max	Average ± SD[a]	*n*	Min	Max	Average ± SD	Min	Max	Average ± SD	Min	Max	Average ± SD	Min	Max	Average ± SD	
January 12–14, 2020 (P1)	8	0.3	1.2	0.9 ± 0.3	8	2.3	4.4	3.1 ± 0.7	1.9	16.5	5.4 ± 3.0	43.5	100	88.4 ± 13.1	4.5	8.3	5.9 ± 1.0	0.2
January 15–21, 2020 (P2)	19	0.2	0.9	0.5 ± 0.2	20	1.9	5.4	3.2 ± 0.7	−4.0	16.8	4.5 ± 4.1	33.5	100	73.5 ± 17.7	1.5	7.4	4.5 ± 1.3	0.05
January 22–29, 2020 (P3)	18	1.0	1.6	1.2 ± 0.2	18	2.2	5.6	3.5 ± 0.9	0.6	13.5	4.8 ± 2.3	53.4	100	92.3 ± 10.5	3.1	6.6	4.6 ± 0.7	1.3

SD[a]: standard deviation.

Table 2
Chemical and isotopic composition of downstream water in each period from 12 January 2020 to 29 January 2020.

Unit	EC				Na^+				Cl^-				$\delta^{18}O$				δD			
	μS/cm				mg/L				mg/L				‰				‰			
Sampling period	*n*	Min	Max	Average ± SD[a]	*n*	Min	Max	Average ± SD	*n*	Min	Max	Average ± SD	*n*	Min	Max	Average ± SD	*n*	Min	Max	Average ± SD
January 12–14, 2020 (P1)	8	34.5	43.1	38.5 ± 2.7	8	1.3	3.1	2.4 ± 0.6	8	3.0	5.0	4.2 ± 0.7	8	−11.26	−10.54	−10.90 ± 0.25	8	−83.26	−78.61	−81.05 ± 1.59
January 15–21, 2020 (P2)	19	40.9	64.9	56.1 ± 7.4	18	1.8	4.5	3.1 ± 0.7	18	3.5	6.9	5.2 ± 1.0	20	−11.29	−10.41	−10.84 ± 0.20	20	−83.68	−77.99	−80.76 ± 1.30
January 22–29, 2020 (P3)	20	38.6	58.3	47.8 ± 6.1	19	1.1	4.2	2.0 ± 0.9	19	3.2	7.3	4.6 ± 1.2	20	−11.39	−10.54	−10.78 ± 0.21	20	−82.90	−78.28	−79.82 ± 1.34

SD[a]: standard deviation.

to −53.7‰ (average of −77.0 ± 13.4‰) and − 89.6‰ to −77.1‰ (average of −84.6 ± 3.1‰), respectively. The mean isotopic values of the stream water were intermediate to those of the groundwater and snow.

Fig. 2f shows the isotopic compositions of the stream water plotted as a function of time. Distinct diel variations with large amplitudes (maximum values of 0.65‰ and 3.95‰; long arrow) were observed for both $\delta^{18}O$ and δD in the stream water samples obtained during the cold period (Period 2). However, the amplitudes of these diel variations diminished to 0‰ and 0.02‰ (short arrows) in the relatively warm summer period (Period 3). In addition, the stable isotope values of the stream water exhibited a similar pattern to the variation in flow velocity (Fig. 2a and f). The isotopic compositions of the stream water were positively correlated with the flow velocity ($r = 0.51$ for $\delta^{18}O$ and $r = 0.59$ for δD). The isotopic compositions of the stream water samples obtained in each period are summarized in Table 2.

4. Discussion

4.1. Stable water isotope characterization and hydrological condition in subpolar regions

Fig. 3 displays the linear relationship between $\delta^{18}O$ and δD for all samples. Also shown are the global meteoric water line (GMWL; $\delta D = 8 \times \delta^{18}O + 10$, Craig, 1961) and the local meteoric water line (LMWL; $\delta D = 7.1 \times \delta^{18}O - 2.2$, Simões et al., 2004) of precipitation samples from the nearest Chile Frei Station, 11 km away from the stream water sampling site. In Fig. 3, the groundwater samples plotted directly on or under the LMWL. The linear trend of the stream water samples ($\delta D = 6.48 \times \delta^{18}O - 10.33$, $R^2 = 0.86$) plotted away from the LMWL, and the lower slope suggests that the sampled water underwent evaporative loss and/or isotopic exchange between the liquid water and ice by melting (Dansgaard, 1964; Lee et al., 2010b; Jung et al., 2021). These observations indicate that the groundwater and stream water in the study area are meteoric in origin, and a certain amount of evaporation and isotopic exchange during melting may have occurred between the liquid water and ice inside the snow or ice before and/or during hydrological processes and transport.

The wide range of isotopic compositions of snow can be attributed to three main factors. The first factor is the isotopic heterogeneity of the snowpack caused by isotopic redistribution in the porewater, ice, and meltwater of the snowpack. Lee et al. (2010b) noted that the isotopic heterogeneity of snowpack could significantly affect the temporal variation in the isotopic composition of meltwater. The second factor is the difference in the origin of the vapor source. It is likely that the isotopically heavier snow originated from water vapor that directly evaporated from the seawater near the study site on the coast of Maxwell Bay, whereas the isotopically depleted snow originated from water transported from a relatively remote location. The third factor is the isotopic fractionation caused by sublimation (and snow age). The stable isotopic compositions of snow can change as a result of the interaction between the atmosphere and the surface of snow cover (Earman et al., 2006; Sokratov and Golubev, 2009).

In snow-dominated headwater catchments, snowmelt is the major source of groundwater recharge and surface water runoff, and its fluxes determine streamflow during the snowmelt season (Woelber et al., 2018). These variations are associated with meteorological factors that drive hydrological responses in snow-dominated headwater catchments (Woelber et al., 2018). Upstream snowmelt that infiltrates the underlying soil and reaches the water table recharges groundwater and discharges downstream. In other words, plentiful snowmelt during summer can promote the continuous replenishment of supra-permafrost water to streamflow in subpolar regions. Additionally, surface runoff (also known as overland flow) occurs when excess snowmelt water can no longer rapidly infiltrate or become sufficiently saturated in the soil. According to previous studies, the runoff contributions of snowmelt and glacier melt are significant compared with those of groundwater during the snowmelt season in permafrost areas (Engel et al., 2016; Paquette et al., 2018).

The snowmelt rate is determined by the fluxes of sensible heat and latent heat, which are influenced by surface meteorological conditions such as air temperature, relative humidity, wind speed, radiation, and the amount of precipitation (Grundstein and Leathers, 1998; Hasebe and Kumekawa, 1995; Lim et al., 2022; Tian et al., 2018). In addition, hydrological processes in permafrost regions can be controlled by the dynamics of the active layer, and it has been reported that the groundwater flux and depth increase with an increase in the active layer thickness (Walvoord et al., 2012; Tetzlaff et al., 2018; Langford et al., 2020). Understanding the variability in the flow path is important for ensuring stream water quality and realizing sustainable management of water supply resources.

4.2. Relationship between the solute concentration (C) and stream discharge (Q)

Solute concentration–stream discharge (C–Q) relationships can provide valuable information regarding hydrological processes in many catchments (Godsey et al., 2009; Kim et al., 2017b; Wlostowski et al., 2018b). To understand how snowmelt in the upstream region moves downstream, we investigated the C–Q relationships for solutes produced primarily by water–rock interactions and atmospheric inputs to snowmelt (Godsey et al., 2009). C–Q

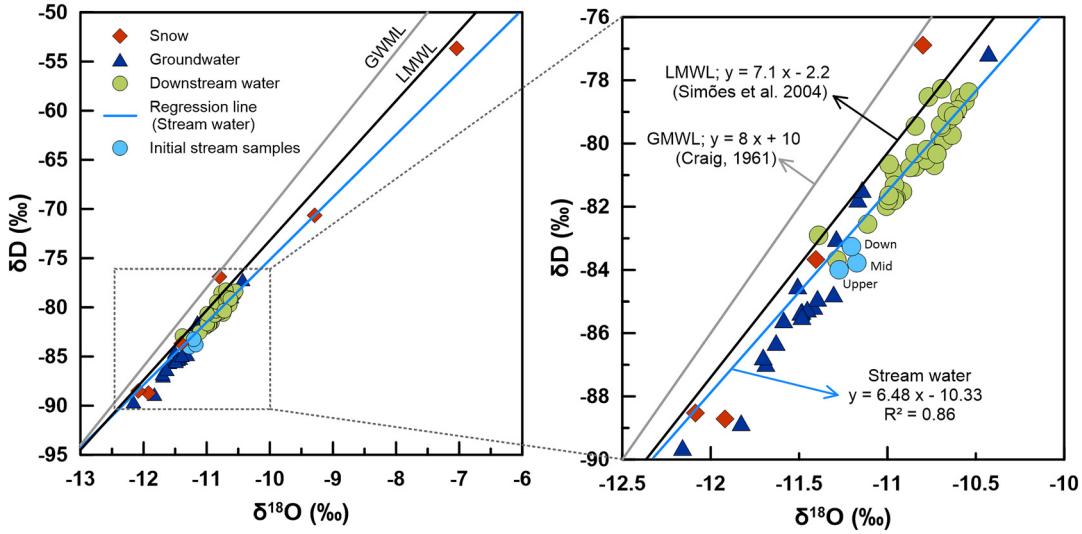

Fig. 3. Stable water composition (δ^2H vs. $\delta^{18}O$, ‰) for snow, groundwater, and stream water samples with the regression line (blue line) corresponding to the stream water samples. GMWL (grey line) denotes the global meteoric water line (Craig, 1961; $\delta D = 8\delta^{18}O + 10$), and LMWL (black line) denotes the local meteoric water line (Simões et al., 2004; $\delta D = 7.1\delta^{18}O - 2.2$).

plots are often linear on logarithmic axes, indicating that a power-law relationship exists between C and Q (i.e., $C = aQ^b$, where a and b are constants). The exponent in this power-law relationship (or equivalently, the slope of the C–Q relationship on logarithmic axes) has a physical interpretation (Godsey et al., 2009). A slope of zero indicates that the chemostatic behavior of a catchment, that is, the solute concentration, remained constant as the discharge varied. In contrast, a slope of −1, indicates that the solute concentration is negatively correlated with the discharge amount, as might be expected if dilution was the dominant process controlling the concentration (Godsey et al., 2009).

Fig. 4 shows the C–Q plots based on the analyzed data. The best-fit log–log C–Q slopes for the major ions varied between approximately −0.09 and − 0.51. Nevertheless, certain solutes, such as Ca^{2+}, Mg^{2+}, and Na^{+}, exhibited statistically weak dilution effects. Both K^{+} and Si^{4+} behave chemostatically for chemical weathering products, with small negative log–log slopes. Although this study showed that the dilution effect of snowmelt, rather than chemical weathering, controls the solute concentrations of the stream water system in the study area, studies have reported the subglacial weathering of silica in other Antarctic regions (Hatton et al., 2020; Hirst et al., 2020). These findings indicate that the solute yield from the catchment was predominantly determined by the water yield during the study period because the solute concentrations remained nearly constant across a wide discharge range.

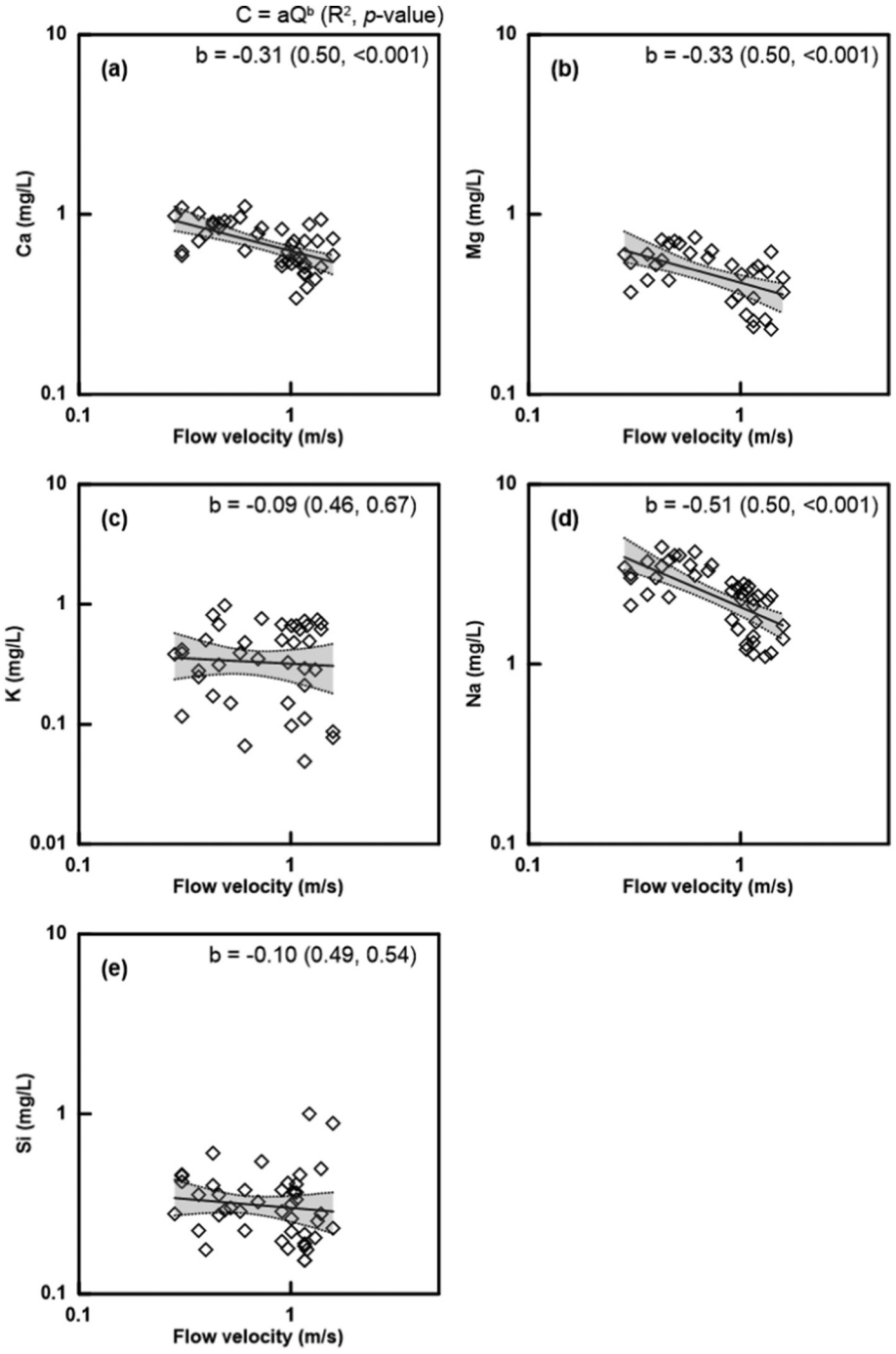

Fig. 4. Concentration–discharge (C–Q) relationships of (a) Ca, (b) Mg, (c) K, (d) Na, and (e) Si. Exponents (b), R^2, and *p*-value of the power law fit to the C–Q relationship for our measurements are shown in each plot.

4.3. Diel variations of hydrological processes at different timescales

There are two possible flow paths through which upstream meltwater can move to the downstream region during the snowmelt period: first, when snowmelt is moved by runoff, and second, when snowmelt is recharged and discharged. These phenomena may occur simultaneously, and according to existing studies, are affected by the active layer. Hence, in this study, we investigated the dynamic fluctuations in flow paths at high resolution using the EC, $\delta^{18}O$, and δD values. If the active layer is frozen and thin, runoff dominates, and the diel isotope signal caused by the difference in the snowmelt rate is transmitted downstream (Lee et al., 2010b; Lee et al., 2020). This phenomenon occurs because the freeze-up period restricts the subsurface flow paths owing to thermal ice growth from both the surface downward and permafrost upward (Tetzlaff et al., 2018). In this case, when the flow increases, the EC values can decrease owing to the dilution effect or increase when the snowmelt concentration is higher than that of stream water (Bales et al., 1989; Feng et al., 2001; Lee et al., 2008; Lee and Jung, 2021). In contrast, the active layer develops and thickens in summer, resulting in an increase in the contribution of old water. In this case, diel variations in isotopic compositions are attenuated in stream water because of an increase in the contribution of old water with homogeneous isotopic compositions. Moreover, the relationship between stream discharge and EC is determined by the water sources with a high contribution rate between groundwater and snow. Specifically, if the

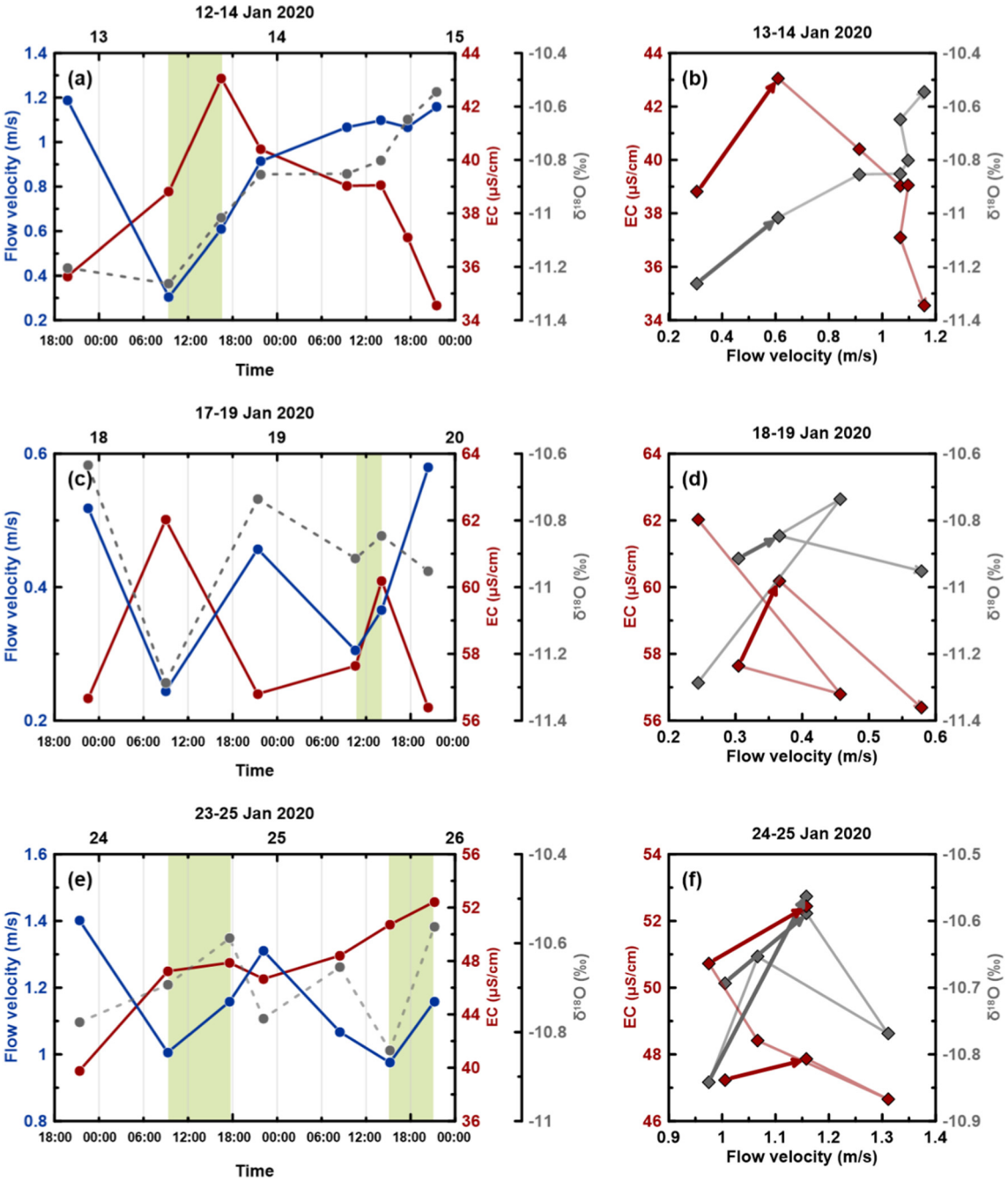

Fig. 5. Temporal variations in flow velocity, EC, and $\delta^{18}O_{H2O}$ and hysteresis pattern progression of EC and $\delta^{18}O_{H2O}$ with the flow velocity. Periods (a, b) 1; (c, d) 2, and (e, f) 3. Green shaded areas indicate periods in which the flow velocity and EC are positively correlated (a, c, and e). Dark arrows represent the evolution of values in the period (b, d, and f) in which the EC and flow velocity are positively correlated.

contribution ratio of snowmelt is higher than that of groundwater, the EC value fluctuates with the same mechanism as previously mentioned; otherwise, the EC value of stream water may vary depending on the fluctuation in the EC value of discharged groundwater. In polar regions, stream and groundwater flows exhibit diel variations during rainless periods, reflecting the addition of meltwater during the snowmelt period in the daytime. These cycles can help clarify the mechanisms of the coupling of meteorological factors and the snowmelt rate to changes in streamflow.

To understand the influence of hydrological flow paths on stream chemistry, high-frequency sampling must be performed to examine the hydrological dynamics within a catchment (Evans and Davies, 1998; Kirchner et al., 2004; Engel et al., 2016). In the case of daily, weekly, or monthly sampling, distinct daily oscillations may remain undiscovered (Kirchner et al., 2004). Based on the observed diel variations in EC, $\delta^{18}O$, and δD values, we attempted to determine the variation in hydrological processes considering the dynamic active layers during austral summer.

In the afternoon of January 12, 2020, at the beginning of the study, the flow velocity of the stream was relatively high (1.2 m/s); however, as the new water input decreased, the flow velocity of the stream rapidly decreased to 0.30 m/s in the morning of January 13 (Fig. 5a). At this time, the EC value increased, likely because the relative proportion of old water increased compared with that in the initial state owing to the baseflow recession moving through the existing active layer as the input of new water decreased. Owing to rainfall in the evening of January 13, the night flow increased to 0.91 m/s and the EC value decreased. In the morning of January 14, the flow was higher than that of the previous day, and the EC value decreased. Subsequently, the flow velocity increased, decreased, and then increased to 1.16 m/s at night, when the EC value decreased, probably as a result of the dilution effect caused by the runoff of new water.

Moreover, a positive correlation was observed between the EC value and flow velocity on the high-frequency scale (Fig. 5b). For example, the flow in the afternoon of January 13 increased slightly to 0.61 m/s compared with that in the morning, and the EC increased as well. This finding indicates that old water or snowmelt with higher EC values than the stream water was discharged into the stream. In general, when snowmelt increases during the daytime, when the temperature is higher than that in the morning, the discharge of old water at higher depths with high EC values may increase due to the infiltration of new water. Additionally, the EC of snowmelt may exhibit irregular fluctuations unrelated to the flow because snowmelt can have a wide range of EC values due to the solute distribution within the snowpack. By combining isotopic and EC data, more confined water sources and flow paths can be identified. Notably, old water has an almost homogeneous isotopic composition, whereas snowmelt, as described above, can have a heterogeneous isotopic composition depending on the degree of fractionation. On January 13, the $\delta^{18}O$ composition of the stream water gradually increased in proportion to the flow velocity without any diel variation (Fig. 5a and b). This finding suggests that meltwater with depleted isotopic values early in the season contributed to the stream as runoff, whereas meltwater was progressively enriched in heavy isotopes owing to isotope fractionation. This indicates that the runoff of new water was a more dominant flow path than the baseflow in this case.

From January 14 to 20, at the beginning of Period 2, the diurnal air temperature variation was large, and the daily mean air temperature gradually decreased. Consequently, the snowmelt rate gradually decreased. In this case, the flow velocity during Period 2 was lower than the mean flow of the entire study period. The average EC value during Period 2 was higher than those during Periods 1 and 3 (Table 2). A positive relationship was observed between the values in the morning and afternoon of January 19; at this time, the $\delta^{18}O$ composition of the stream water also increased. This phenomenon could be attributed to the isotopic evolution of new water (Fig. 5c and d).

Compared with Period 1, the diurnal air temperature difference increased in Period 2, which led to a difference in the snowmelt rate and affected the degree of isotope fractionation, resulting in diel variations with large amplitudes. Such diel variations were clearly observed on January 14–16 and 17–19, corresponding to the early and mid-stages of Period 2, respectively. In particular, the amplitude of the largest diel variation in isotopes during the study period was observed between the night of January 17 and morning of January 18 (Fig. 5c). At this time, the diel variation was caused by isotopic fractionation between snow and liquid water. From the previous night to the next morning, considerable isotopic fractionation occurred at a low snowmelt rate under a low atmospheric temperature, and meltwater with a relatively depleted isotopic composition was produced. As the afternoon progressed, the snowmelt rate gradually increased due to the increase in the atmospheric temperature, resulting in less fractionation, and thus, the meltwater was similar to snow with the heavy isotope composition. Notably, the $\delta^{18}O$ composition of the daily stream water samples exhibited a sine function over time. The diel variation signal of the stable isotopic compositions of new water, clearly observed in the stream, indicated that runoff was the dominant flow path due to the decreased thickness of the active layer. Although certain periods exhibited large diurnal temperature differences in Period 3, the diel variation was relatively small, as discussed in the subsequent text.

In Period 3, the daily mean air temperature was higher than that in Period 2 (Table 1). A mild air temperature with a small diurnal difference increased the amount of snowmelt and flow velocity of the stream. Moreover, the EC value gradually decreased as the flow velocity rapidly increased from January 22 to 23 at the beginning of Period 3, as in Period 2. The $\delta^{18}O$ compositions of the stream water also increased in proportion to the flow velocity, likely because of the gradual isotopic differentiation due to a relatively constant snowmelt rate with a small diurnal air temperature difference, as in Period 1 (from January 13 to 15). In contrast, on January 24 and 25, a positive correlation was observed, and the EC value increased as the flow velocity increased, likely owing to the presence of old or new water with higher EC values than the stream water (Fig. 5e and f). This phenomenon can be clearly distinguished by considering the observed isotopic compositions. In the afternoon, as the flow increased, the $\delta^{18}O$ compositions of the stream water also increased (Fig. 5e and f). The contribution of new water likely influenced the variations in the chemical and stable isotopic compositions. Additionally, from January 25 to 28, as the air diurnal temperature difference increased, the difference in the amount of snowmelt during the day and night led to diel variations in the stable isotope values, as in Period 2. However, the amplitudes of the diel variations in the stable isotopic compositions of the stream water at this time were smaller than those in Period 2. As mentioned previously, the diel variation signal in the stable isotopic compositions of stream water may be attenuated due to the increase in the contribution of old water following the development of the active layer. However, this does not apply in this case because if the contribution of old water increases, the EC value should increase, whereas it decreased in Period 3 compared with Period 2. Therefore, the attenuation of this diel variation signal in the stream was related to the diel variation of new water with a low amplitude in terms of its isotopic composition, and the contribution of new water was still larger than that of old water.

5. Conclusions

This study can provide novel insights into the dynamics of hydrologic flow paths during the snowmelt season in maritime Antarctica, a topic that has not been widely addressed in existing studies. We found that the stream is part of catchment dominated by new water because diel variations in isotopic compositions were observed during summer periods. However, there was a difference in the hydrological characteristics between cold and warm summer periods. During the summer with cold events, as the snowmelt rate decreased, the amount of new water decreased (Fig. 6a). Hence, the EC value increased because the contribution of old water (supra-permafrost groundwater) increased compared with that in the initial state (Fig. 6b). During these periods, diel variations in the stable isotopic compositions of new water were clearly observed in the stream water, indicating that runoff was the dominant flow path (Fig. 6c). In the summer with warm events, the amount of snowmelt increased (Fig. 6d) and the EC value

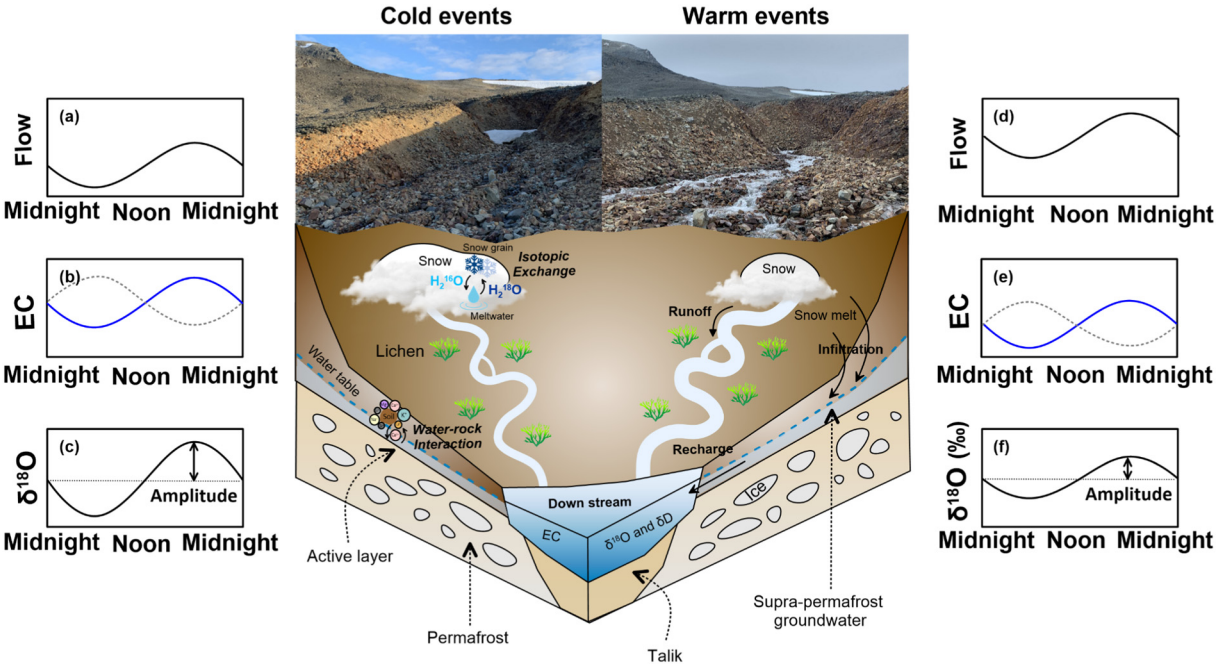

Fig. 6. Conceptual schematic of the hydrologic pathway through the relationship between streamflow and EC or $\delta^{18}O_{H2O}$ in summer with cold events and warm events, respectively. (a) a relatively low stream flow with diel variation; (b) a relatively high EC in the stream water showing a negative (dotted grey) and positive (blue) relationship with stream flow; (c) the isotopic variation with a relatively large diel variation; (d) a relatively high stream flow with diel variation; (e) a relatively low EC in the stream water showing a negative (dotted grey) and positive (blue) relationship with stream flow; (f) the isotopic variation with a relatively low diel variation.

decreased owing to the dilution effect (Fig. 6e). In addition, the diel variations in the stable isotopic compositions of the stream water were attenuated compared with those in the cold summer (Fig. 6f). Based on the low EC value, these observations were not due to the increased contribution of old water, but rather the contribution of new water with a low amplitude signal in the diel variations of stable isotopes. It is expected that KGI will experience major changes due to climatic warming, which could impact the active layer thickness, weathering processes, and export to downstream ecosystems. Therefore, understanding the present process is fundamental for predicting what changes may occur in the future. Although this study was able to identify diel variations in meltwater over a relatively short period, long-term monitoring is needed to investigate hydrological pathways and water-related ecosystems for climate-related changes in subpolar catchments.

CRediT authorship contribution statement

H. Jung: investigation, visualization, writing-original draft preparation; **S. Jeen:** methodology, writing-review and editing; **H. Lee:** resources, writing-review; **J. Lee:** investigation, writing-review and editing. All authors have read and agreed to the published version of manuscript.

Declaration of competing interest

The authors declare that they have no known competing financial interests or personal relationships that could have appeared to influence the work reported in this paper.

Acknowledgments

This work was financially supported by research grants (PE21130) from the Korea Polar Research Institute. This work was also partially supported by three other research grants: one from the Korea Ministry of Oceans and Fisheries (KIMST20190361), another from the National Research Council of Science and Technology (NST) grant of the Korean government (MSIP) (CAP-17-05-KIGAM) and the other from the Basic Science Research Program through the National Research Foundation of Korea (NRF) funded by the Ministry of Education (2021R1A6A3A13043968).

Appendix A. Supplementary data

Supplementary data to this article can be found online at https://doi.org/10.1016/j.scitotenv.2022.153784.

References

Bales, R.C., Davis, R.E., Stanley, D.A., 1989. Ion elution through shallow homogeneous snow. Water Resour. Res. 25, 1869–1878.
Birkel, C., Soulsby, C., Tetzlaff, D., Dunn, S., Spezia, L., 2012. High-frequency storm event isotope sampling reveals time-variant transit time distributions and influence of diurnal cycles. Hydrol.Process. 26 (2), 308–316.
Biskaborn, B.K., Smith, S.L., Noetzli, J., et al., 2019. Permafrost is warming at a global scale. Nat. Commun. 10, 264.
Cano-Paoli, K., Chiogna, G., Bellin, A., 2019. Convenient use of electrical conductivity measurements to investigate hydrological processes in Alpine headwaters. Sci. Total Environ. 685, 37–49.
Chang, S.K., Kim, D.Y., Lee, B.Y., Chung, H.S., 1990. Environment around King Sejong station, King George Island, Antarctica in 1988/89. Korean J.Polar Res. 1, 59–65.
Cho, S.M., Lee, H., Hong, S.G., Lee, J., 2020. Study of ecophysiological responses of the Antarctic fruticose lichen Cladonia borealis using the PAM fluorescence system under natural and laboratory conditions. Plants 9 (1), 85.
Chun, H.Y., Chang, S.K., Lee, J.I., 1994. Biostratigraphic study on the plant fossils from the Barton Peninsula and adjacent area. J. Paleont. Soc. Korea 10, 69–84.
Cooper, L.W., Olsen, C.R., Solomon, D.K., Larsen, I.L., Cook, R.B., Grebmeier, J.M., 1991. Stable isotopes of oxygen and natural and fallout radionuclides used for tracing runoff during snowmelt in an arctic watershed. Water Resour. Res. 27, 2171–2179.
Craig, H., 1961. Isotopic variations in meteoric waters. Science 133 (3465), 1702–1703.
Dansgaard, W., 1964. Stable isotopes in precipitation. Tellus 16 (4), 436–468.
Earman, S., Campbell, A.R., Phillips, F.M., Newman, B.D., 2006. Isotopic exchange between snow and atmospheric water vapor: estimation of the snowmelt component of groundwater recharge in the southwestern United States. J. Geophys. Res. 111, D09302.
Engel, M., Penna, D., Bertoldi, G., Dell'Agnese, A., Soulsby, C., Comiti, F., 2016. Identifying run-off contributions during melt-induced run-off events in a glacierized alpine catchment. Hydrol. Process. 30, 343–364.
Evans, C., Davies, T.D., 1998. Causes of concentration/discharge hysteresis and its potential as a tool for analysis of episode hydrochemistry. Water Resour. Res. 34, 129–137.

Falk, U., López, D.A., Silva-Busso, A., 2018. Multi-year analysis of distributed glacier mass balance modelling and equilibrium line altitude on King George Island, Antarctic Peninsula. The Cryosphere 12, 1211–1232.
Feng, X., Kirchner, J.W., Renshaw, C.E., Osterhuber, R.S., Klaue, B., Taylor, S., 2001. A study of solute transport mechanisms using rare earth element tracers and artificial rainstorms on snow. Water Resour. Res. 37, 1425–1435.
Fouché, J., Bouchez, C., Keller, C., Allard, M., Ambrosi, J.-P., 2021. Seasonal cryogenic processes control supra-permafrost pore water chemistry in two contrasting cryosols. Geoderma 401, 115302.
Godsey, S.E., Kirchner, J.W., Clow, D.W., 2009. Concentration-discharge relationships reflect chemostatic characteristics of US catchments. Hydrol. Process. 23, 1844–1864.
Grundstein, A.J., Leathers, D.J., 1998. A case study of the synoptic patterns influencing midwinter snowmelt across the northern Great Plains. Hydrol. Process. 12, 2293–2305.
Hasebe, M., Kumekawa, T., 1995. Estimation of snowmelt volume using air temperature and wind speed. Environ. Int. 21, 497–500.
Hatton, J.E., Hendry, K.R., Opfergelt, S., et al., 2020. Silicon isotopic composition of dry and wet-based glaciers in Antarctica. Front. Earth Sci. 8 (286).
Hinkler, J., Hansen, B.U., Tamstorf, M.P., Sigsgaard, C., Petersen, D., 2008. Snow and snowcover in central Northeast Greenland. In: Meltofte, H., Christensen, T.R., Elberling, B., Forchhammer, M.C., Rasch, M. (Eds.), High-Arctic Ecosystem Dynamics in a Changing Climate. Advances in Ecological Research. 40, pp. 175–195.
Hirst, C., Opfergelt, S., Gaspard, F., et al., 2020. Silicon isotopes reveal a non-glacial source of silicon to Crescent Stream, McMurdo Dry Valleys, Antarctica. Front. Earth Sci. 8 (229).
Hrbáček, F., Vieira, G., Oliva, M., et al., 2021. Active layer monitoring in Antarctica: An overview of results from 2006 to 2015. Polar Geo. 44 (3), 217–231.
Hur, S.D., Lee, J.I., Hwang, J., Choe, M.Y., 2001. K-Ar age and geochemistry of hydrothermal alteration in the Barton Peninsula, King George Island,Antarctica. Ocean Polar Res. 23, 11–21.
Hussainzada, W., Lee, H.S., Vinayak, B., Khpalwak, G.F., 2021. Sensitivity of snowmelt runoff modelling to the level of cloud coverage for snow cover extent from daily MODIS product collection 6. J.Hydrol.Reg.Stud. 36, 100835.
Jung, H., Koh, D.-C., Kim, Y.S., Jeen, S.-W., Lee, J., 2020a. Stable isotopes of water and nitrate for the identification of groundwater flowpaths: a review. Water 12, 138.
Jung, Y.Y., Koh, D.-C., Lee, J., Tsujimura, M., Yun, S.T., Lee, K.-S., 2020b. Mean transit time and subsurface flow paths in a humid temperate headwater catchment with granitic bedrock. J. Hydrol. 587, 124942.
Jung, H., Kim, Y.S., Yoo, J., Park, B., Lee, J., 2021. Seasonal variations in stable nitrate isotopes combined with stable water isotopes in a wastewater treatment plant: implications for nitrogen sources and transformation. J. Hydrol. 599, 126488.
Kennedy, A.D., 1993. Water as a limiting factor in the Antarctic terrestrial environment: a biogeographical synthesis. Arctic Alp Res 25, 308–315.
Kim, H., Cho, S.H., Lee, D., Jung, Y.Y., Kim, Y.H., Koh, D.C., Lee, J., 2017a. Influence of preevent water on streamflow in a granitic watershed using hydrograph separation. Environ. Earth Sci. 76, 82.
Kim, H., Dietrich, W.E., Thurnhoffer, B.M., Bishop, J.K.B., Fung, I.Y., 2017b. Controls on solute concentration-discharge relationships revealed by simultaneous hydrochemistry observations of hillslope runoff and stream flow: the importance of critical zone structure. Water Resour. Res. 53, 1424–1443.
Kim, H., Lee, J.I., Choe, M.Y., Cho, M., Zheng, X., Sang, H., Qin, J., 2000a. Geochronologic evidence for Early Cretaceous volcanic activity on Barton Peninsula, King George Island, Antarctica. Polar Res. 19, 251–260.
Kim, J., Jeen, S.-W., Lim, H.S., Lee, J., Kim, O.-S., Lee, H., Hong, S.G., 2020b. Hydrogeological characteristics of groundwater and surface water associated with two small lake systems on King George Island,Antarctica. J. Hydrol. 590, 125537.
Kirchner, J.W., Feng, X., Neal, C., Robson, A.J., 2004. The fine structure of water-quality dynamics: the(high-frequency) wave of the future. Hydrol. Process. 18, 1353–1359.
Klaus, J., McDonnell, J.J., 2013. Hydrograph separation using stable isotopes: review and evaluation. J. Hydrol. 505, 47–64.
Langford, J.E., Schincariol, R.A., Nagare, R.M., Quinton, W.L., Mohammed, A.A., 2020. Transient and transition factors in modeling permafrost thaw and groundwater flow. Groundwater 58, 258–268.
Lee, J., Jung, H., 2021. Understanding the relationship between meltwater discharge and solute concentration by modeling solute transport in a snowpack in snow-dominated regions – a review. Polar Sci. 100782.
Lee, J.I., Hwang, J., Kim, H., Kang, C.Y., Lee, M.J., Nagao, K., 1996. Subvolcanic zoned granitic pluton in the Barton and Weaver peninsulas, King George Island,Antarctica. Proc. NIPR Symp. Antarctic Geosci. 9, pp. 76–90.
Lee, J.I., Hur, S.D., Yoo, C.M., Yeo, J.P., Kim, H., Hwang, J., Choe, M.Y., Nam, S.H., Kim, Y., Park, B.-K., Zheng, X., López-Martinez, J., 2001. Explanatory Text of the Geologic Map of Barton And Weaver Peninsulas, King George Island, Antarctica. Korea Ocean Research and Development Institute, p. 28.
Lee, Y.I., Lim, H.S., Yoon, H.I., 2004. Geochemistry of soils of King George Island, South Shetland Islands, West Antarctica: implications for pedogenesis in cold polar regions. Geochim. Cosmochim. Acta 68, 4319–4333.
Lee, J., Feng, X., Posmentier, E.S., Faiia, A.M., Osterhuber, R., Kirchner, J.W., 2008. Modeling of solute transport in snow using conservative tracers and artificial rain-on-snow experiments. Water Resour. Res. 44, W02411.
Lee, J., Feng, X., Faiia, A., Posmentier, E., Osterhuber, R., Kirchner, J., 2010a. Isotopic evolution of snowmelt: a new model incorporating mobile and immobile water. Water Resour. Res. 46, W11512.
Lee, J., Feng, X., Faiia, A.M., Posmentier, E.S., Kirchner, J.W., Osterhuber, R., et al., 2010b. Isotopic evolution of a seasonal snowcover and its melt by isotopic exchange between liquid water and ice. Chem. Geol. 270, 126–134.
Lee, J., Hur, S.D., Lim, H.S., Jung, H., 2020. Isotopic characteristics of snow and its meltwater over the Barton Peninsula,Antarctica. Cold Reg. Sci. Technol. 173, 102997.
Leishman, M., Wild, C., 2001. Vegetation abundance and diversity in relation to soil nutrients and soil water content in Vestfold Hills,East Antarctica. Antarct. Sci. 13 (2), 126–134.
Lim, H.S., Park, Y., Lee, J.-Y., Yoon, H.I., 2014. Geochemical characteristics of meltwater and pondwater on Barton and Weaver Peninsulas of King George Island,West Antarctica. Geochem. J. 48 (4), 409–422.
Lim, H.S., Kim, H.-C., Kim, O.-S., Jung, H., Lee, J., Hong, S.G., 2022. Statistical understanding for snow cover effects on near-surface ground temperature at the margin of maritime Antarctica, King George Island. Geoderma 410.
McGuire, K.J., McDonnell, J.J., 2006. A review and evaluation of catchment transit time modeling. J. Hydrol. 330, 543–563.
McGuire, K., McDonnell, J.J., 2007. Stable isotope tracers in watershed hydrology. In: Michener, R., Lajtha, K. (Eds.), Stable Isotopes in Ecology And Environmental Science, 2nd ed. Wiley/Blackwell, Malden, MA, USA, pp. 334–540.
Mook, W., Groeneveld, D., Brown, A., Van Ganswijk, A., 1974. Analysis of a runoff hydrograph by means of natural 18O. Isotope Techniques in Groundwater Hydrology. International Atomic Energy Agency, Vienna, pp. 145–156.
Muñoz-Villers, L.E., McDonnell, J.J., 2012. Runoff generation in a steep, tropical montane cloud forest catchment on permeable volcanic substrate. Water Resour. Res. 48 (9), W09528.
Pankhurst, R.J., Smellie, J.L., 1983. K-Ar geochronology of the South Shetland Islands, Lesser Antarctica: apparent lateral migration of Jurassic to Quaternary island arc volcanism. Earth Planet. Sci. Lett. 66, 214–222.
Paquette, M., Fortier, D., Vincent, W.F., 2018. Hillslope water tracks in the High Arctic: seasonal flow dynamics with changing water sources in preferential flow paths. Hydrol. Process. 32, 1077–1089.
Park, B.-K., 1989. Potassium-argon radiometric ages of volcanic and plutonic rocks from the Barton Peninsula, King George Island,Antarctica. J. Geol. Soc. Korea 25, 495–497.
Qiu, J., 2012. Thawing permafrost reduces river runoff. Nature https://doi.org/10.1038/nature.2012.9749.
Rango, A., Martinec, J., 1995. Revisiting the degree-day method for snowmelt computations. J. Am. Water Resour. Assoc. 31 (4), 657–669.
Simões, J.C., Ferron, F.A., Bernardo, R.T., Aristarain, A.J., Stievenard, M., Pourchet, M., Delmas, R.J., 2004. Ice core study from the King George Island, South Shetlands, Antarctica. Pesqui. Antart. Bras. 4, 9–23.
Sjöberg, Y., Jan, A., Painter, S.L., Coon, E.T., Carey, M.P., O'Donnell, J.A., Koch, J.C., 2021. Permafrost promotes shallow groundwater flow and warmer headwater streams. Water Resour. Res. 57, e2020WR027463.
Sklash, M.G., Farvolden, R.N., Fritz, P., 1976. A conceptual model of watershed response to rainfall, developed through the use of oxygen-18 as a natural tracer. Can. J. Earth Sci. 13 (2), 271–283.
Smellie, J.L., Pankhurst, R.J., Thomson, M.R.A., Davies, R.E.S., 1984. The Geology of the South Shetland Islands: VI. Stratigraphy, Geochemistry And Evolution. Scientific Report 87. British Antarctic Survey.
Sokratov, S.A., Golubev, V.N., 2009. Snow isotopic content change by sublimation. J. Glaciol. 55 (193), 823–828.
Stammerjohn, S.E., Scambos, T.A., 2020. Warming reaches the South Pole. Nat. Clim. Chang. 10, 710–711.
Taylor, S., Feng, X., Kirchner, J.W., Osterhuber, R., Klaue, B., Renshaw, C.E., 2001. Isotopic evolution of a seasonal snowpack and its melt. Water Resour. Res. 37, 759–769.
Tetzlaff, D., Piovano, T., Ala-Aho, P., Smith, A., Carey, S.K., Marsh, P., et al., 2018. Using stable isotopes to estimate travel times in a data-sparse Arctic catchment: challenges and possible solutions. Hydrol. Process. 32, 1936–1952.
Throckmorton, H.M., Newman, B.D., Heikoop, J.M., Perkins, G.B., Feng, X., Graham, D.E., et al., 2016. Active layer hydrology in an arctic tundra ecosystem: quantifying water sources and cycling using water stable isotopes. Hydrol. Process. 30, 4972–4986.
Tian, L., Li, H., Li, F., Li, X., Du, X., Ye, X., 2018. Identification of key influence factors and an empirical formula for spring snowmelt-runoff: a case study in mid-temperate zone of northeast China. Sci. Rep. 8, 16950.
Walvoord, M.A., Voss, C.I., Wellman, T.P., 2012. Influence of permafrost distribution on groundwater flow in the context of climate-driven permafrost thaw: example from Yukon Flats Basin, Alaska,United States. Water Resour. Res. 48, W07524.
Wlostowski, A.N., Gooseff, M.N., McKnight, D.M., Lyons, W.B., 2018. Transit times and rapid chemical equilibrium explain chemostasis in glacial meltwater streams in the McMurdo Dry Valleys, Antarctica. Geophys. Res. Lett. 45, 13322–13331.
Woelber, B., Maneta, M.P., Harper, J., Jencso, K.G., Gardner, W.P., Wilcox, A.C., et al., 2018. The influence of diurnal snowmelt and transpiration on hillslope throughflow and stream response. Hydrol. Earth Syst. Sci. 22, 4295–4310.
Woo, M., 2012. Permafrost Hydrology. Springer, Berlin Heidelberg, Berlin.
Yoo, C.M., Choe, M.Y., Jo, H.R., Kim, Y., Kim, K.H., 2001. Volcaniclastic sedimentation of the Sejong Formation (Late Paleocene-Eocene), Barton Peninsula, King George Island, Antarctica. Ocean Polar Res. 23, 97–107.